

Article

## Synthesis and Optical Study of a New Oligophenylene

Sarra Ben Amor <sup>1</sup>, Ayoub Haj Said <sup>1,\*</sup>, Mourad Chemek <sup>2</sup>, Florian Massuyeau <sup>3</sup>, Jany Wéry <sup>3</sup>, Eric Faulques <sup>3</sup>, Kamel Alimi <sup>2</sup> and Sadok Roudesli <sup>1</sup>

<sup>1</sup> Laboratoire Polymères, Biopolymères, Matériaux Organiques, Faculté des sciences, Université de Monastir, Boulevard de l'environnement, 5000, Tunisia;

E-Mails: sarra\_ben\_amor@yahoo.fr (S.B.A.); sadok.roudesli@fsm.rnu.tn (S.R.)

<sup>2</sup> Unité de Recherche, Matériaux Nouveaux et Dispositifs Electroniques Organiques, Faculté des Sciences, Université de Monastir, Boulevard de l'environnement, 5000 Monastir, Tunisia;

E-Mails: chmek\_mourad@yahoo.fr (M.C.); kamel.alimi@fsm.rnu.tn (K.A.)

<sup>3</sup> Institut des Matériaux Jean Rouxel, Université de Nantes, CNRS, UMR 6502, 2 rue de la Houssinière, B.P. 32229, 44322 Nantes, Cedex 03, France;

E-Mails: florian.massuyeau@cnrs-immn.fr (F.M.), jany.wery@cnrs-immn.fr (J.W.);

eric.faulques@cnrs-immn.fr (E.F.)

\* Author to whom correspondence should be addressed; E-Mail: ayoub.hajsaid@fsm.rnu.tn; Tel.: +216-735-002-76; Fax: +216-735-002-78.

Received: 16 April 2012; in revised form: 10 May 2012 / Accepted: 14 May 2012 /

Published: 31 May 2012

---

**Abstract:** A new substituted oligophenylene was prepared by the Knoevenagel condensation of 4-methoxybenzaldehyde with a functionalized oligophenylene (OMPA). The latter was obtained by (4-methoxy phenyl) acetonitrile electrochemical oxidation. The resulting modified oligomer was characterized by various spectroscopic techniques: NMR, FTIR and UV. The thermal study showed that the modified material exhibited a lower thermal stability compared with OMPA. Finally, the optical study revealed that in solution, the emission was red-shifted when compared with the non-modified oligomer emission and that the optical gap changed from 3.1 eV to 2.75 eV. In thin layer solid state, photoluminescence was again red-shifted by 120 nm, which is probably due to an interaction between the oligomer chains. In addition, a transient photoluminescence study was undertaken for the synthesized materials. It showed that the lifetimes of the photo-generated species were shortened by the conjugation extension in the modified oligomer and by the inter-chain interactions in the solid state.

**Keywords:** conjugated polymers; oligophenylenes; photoluminescence

---

## 1. Introduction

Conjugated polymers have attracted much attention because of their promising electronic, opto-electronic and electrochemical properties. These polymers have applications in various technological fields, such as the elaboration of photovoltaic devices, electroluminescent displays, field-effect transistors, active thin layers of different sensing devices, supercapacitors *etc.* [1–4]. Actually, semiconducting polymers have many advantages when compared with inorganic semiconductors. They offer a greater flexibility and adaptability, simple manufacturing techniques and a low cost of production. Moreover, they allow an easier and a better modification of the polymer's physical and chemical properties by making small structural changes in the monomer [4–12]. Indeed, these properties are dependent not only on the nature of the polymeric backbone but also on the presence of covalently attached functional groups. In fact, the modification of the monomer repeat unit or the attachment of functional groups onto the polymer backbone in a post-polymerization step can be used to achieve molecular level control of the structure and the properties of the polymer. Thus, it will be possible to (a) enhance the delocalization of electrons through the  $\pi$ -conjugation on the polymer, (b) improve the optical and electrical properties, (c) give new functionalities to the polymer, and (d) reduce the polymer's band gap by the control of the HOMO-LUMO energy level [4–15].

In this frame, one significant design approach towards low band gap polymers is to introduce rigid and planar units, such as molecules with fused ring structures, into the polymer backbones [16,17]. Generally, these fused components are structurally planar and lead to a substantive extension of conjugation in the polymers [18,19]. Another powerful approach towards designing low band gap polymers is to have alternating donor and acceptor units along the polymer backbone [20–23].

In this study, we report the synthesis and the physicochemical characterization of a new conjugated oligomer prepared by the Knoevenagel condensation of a functionalized oligophenylene (OMPA) with the 4-methoxybenzaldehyde. The material obtained can be described as an oligophenylene backbone with 4-methoxy cyanostyryl pendent chains. Finally, an optical study of the elaborated material will be described.

## 2. Experimental Section

### 2.1. Chemicals

4-Methoxyphenyl acetonitrile, 4-methoxybenzaldehyde and tetraethyl ammonium tetrafluoroborate were from ACROS. Chloroform and dichloromethane were from PROLABO. Diethyl ether, ethanol, petroleum ether and acetonitrile were from PANREAC. Chemicals were used as received.

## 2.2. Analysis

### 2.2.1. Spectroscopic Analysis

FTIR analysis was performed with a Bruker Vector 22. The spectra were obtained with KBr pressed pellets.  $^1\text{H}$  NMR and  $^{13}\text{C}$  NMR spectral data were obtained on a Bruker AV 300 spectrometer in  $\text{CDCl}_3$  as solvent. UV-Vis spectrophotometric measurements were performed with a Shimadzu spectrophotometer. The spectra deconvolution was performed with Origin software.

### 2.2.2. Gel permeation Chromatography (GPC) and Osmometry Analysis

The oligomer chain length was determined by Gel permeation chromatography (GPC) and osmometry. A  $\mu$  styragel 500 A–15  $\mu\text{m}$  column (length 300 mm and diameter 7.8 mm) was used in GPC. The temperature was 30 °C. The solvent was tetrahydrofuran with a flow rate of 0.85 mL/min. Polystyrene was used as a standard for the column calibration. For the osmometry study, a Knauer thermoelectric apparatus was used with the (4-methoxy phenyl) acetonitrile as standard.

### 2.2.3. Thermal Study

A METTLER DSC was used for the thermal study. The samples were analyzed between ambient temperature and 500 °C with a heating rate of 10 °C/min. The dynamic thermogravimetric analysis was carried out in a Perkin-Elmer TGS-1 thermal balance with a Perkin-Elmer UV-1 temperature program control. The samples were placed in a platinum sample holder and the thermal degradation measurements were carried out between 30 and 550 °C at a speed rate of 10 °C/min under nitrogen.

### 2.2.4. Photoluminescence Study

Optical density measurements were carried out at room temperature (RT) using a Cary 2300 spectrophotometer, in the range 200 to 2200 nm. Steady-state photoluminescence emission (PL) was carried out on a Jobin-Yvon Fluorolog 3 spectrometer using a Xenon lamp (500 W) at RT.

Ultrafast photoluminescence experiments were carried out with the regenerative amplified femtosecond laser system installed in Nantes (Hurricane X, Spectra-Physics) delivering 100 fs pulses of wavelength 800 nm at 1 kHz. The samples were excited at  $\lambda_{\text{exc}} = 267$  nm (4.64 eV) by harmonic generation of the Ti:Sapphire laser line in a SHG/THG box. The pump energy pulse is controlled to ensure that excitation density in the samples does not exceed  $10^{17}$   $\text{cm}^{-3}$  to avoid annihilation and sample degradation. The transient PL was spectrally dispersed into an ORIEL MS260i imaging spectrograph (150 grooves/mm,  $f = 1/4$ ) designed to minimize stray light with high spectral resolution. Spectral calibration was performed by entering weak signals at 267 nm and 534 nm in the spectrometer during acquisition through an EKSPLA filter No bc3. These laser lines could also be removed by using an EKSPLA filter No bc4. The time-resolved emission spectra were detected with a high dynamic range HAMAMATSU C7700 streak camera of temporal resolution 20 ps.

### 2.2.5. Electrochemical Techniques

The voltammetric study was performed with a Voltalab10 apparatus from Radiometer driven by the Volta Master software. The working electrode was a 2 mm diameter platinum disk; the reference electrode was a SCE (Tacussel SR110) and the counter electrode was a platinum wire. The preparative electrolyses were carried out in a two-compartment cell, under nitrogen, at a controlled potential versus a SCE (Tacussel C12). The potentiostat and the current integrator were Tacussel (PRT 1-100 and IG 5 respectively). The working electrode and the counter electrode were a 4 cm<sup>2</sup> and a 0.25 cm<sup>2</sup> platinum gauze, respectively. The separation between cell compartments was realized by a number 4 glass frit.

The  $E_{\text{HOMO}}$  and the  $E_{\text{LUMO}}$  were calculated according the empirical method [24,25], where:  $E_{\text{HOMO}}$  (eV) =  $-(E_{\text{onset}}^{\text{oxi}} + 4,4)$  and  $E_{\text{LUMO}}$  (eV) =  $-(E_{\text{onset}}^{\text{red}} + 4,4)$  with the onset potentials were measured vs. an ECS electrode.

## 2.3. Synthesis

### 2.3.1. OMPA Synthesis

OMPA was prepared by preparative electrolyses carried out at a constant potential of 1.8 V. The supporting electrolyte used was tetraethyl ammonium tetrafluoroborate (NEt<sub>4</sub>BF<sub>4</sub>) and the (4-methoxy phenyl) acetonitrile (MPA) concentration was about 0.1 M. Homogenization of the solution was assured by mechanical stirring. The electrolyses were stopped after consumption of 2 F/mole of the starting material. The electrolysis solutions were evaporated under vacuum until elimination of the major part of the acetonitrile, then 50 mL of water was added and an extraction with dichloromethane was performed to eliminate the supporting salt. The organic phase, containing the electrolysis products, was concentrated and then precipitated in diethyl ether. OMPA was collected by filtration as a brown powder. The weight ratio of the powder to the starting material ( $m_p/m_0$ ) was around 0.3.

### 2.3.2. Synthesis of (Z)-2,3-bis(4-methoxyphenyl)acrylonitrile (BMPA)

A 50 mL reaction vessel was equipped with a magnetic stirrer, reflux condenser, gas inlet and a rubber septum. It was charged with 1 mmol of MPA dissolved in 20 mL of anhydrous ethanol. To this mixture was added drop-wise, with stirring, 5 mL of a solution of sodium ethanolate (2 M) and then 0.12 mL of 4-methoxybenzaldehyde. The reaction was controlled by thin layer chromatography. When the reaction was over, the mixture was cooled in an ice bath, then BMPA precipitated as a yellow powder and it was removed by filtration and washed with distilled water and then by ethanol. To purify this product, it was taken in chloroform and precipitated in petroleum ether. The yield of the reaction is 67%. mp 105 °C; <sup>1</sup>H NMR (300 Hz, CDCl<sub>3</sub>) 3.85 (3H, s), 3.87 (3H, s), 6.94–7.87 (9H, m), <sup>13</sup>C NMR (300 MHz, CDCl<sub>3</sub>) 55.48, 108.4, 114.37, 114.42, 118.74, 126.79, 127.12, 127.40, 130.94, 139.99, 160.14 and 161.12. GC-MS-m/z: [M<sup>+</sup>] 265.

### 2.3.3. Oligo BMPA (OBMPA) Synthesis

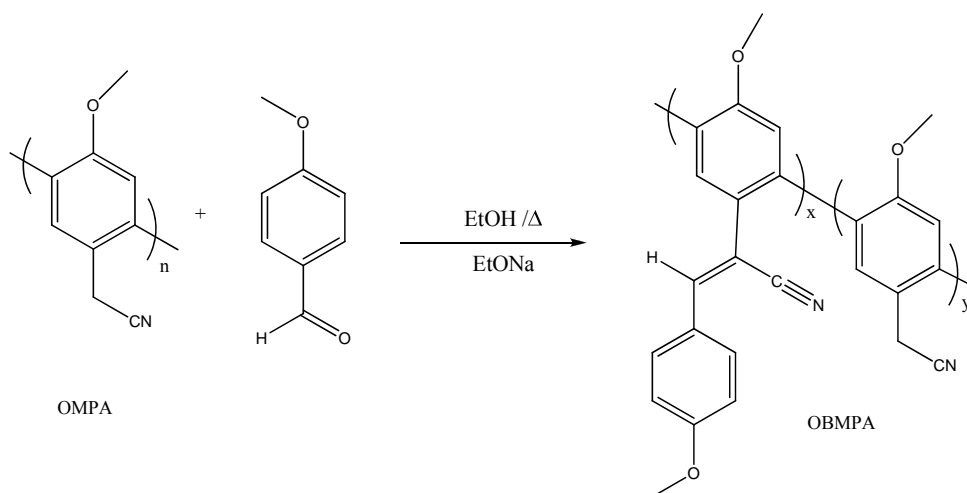
A 50 mL reaction vessel was equipped with a magnetic stirrer, reflux condenser, gas inlet and a rubber septum. It was charged with 145 mg of OMPA dissolved in 20 mL of anhydrous ethanol. To this mixture was added drop-wise, with stirring, 5 mL of a solution of sodium ethanolate (2 M) and then 1.2 mL ( $10^{-3}$  M) of 4-methoxybenzaldehyde. The mixture was refluxed and stirred under Argon atmosphere for 24 h. The OBMPA was precipitated in diethyl ether. The yield was about 65%. The oligomer obtained exhibits good solubility in commonly used solvents ( $\text{CHCl}_3$ ,  $\text{CH}_2\text{Cl}_2$ , THF...).

## 3. Results and Discussion

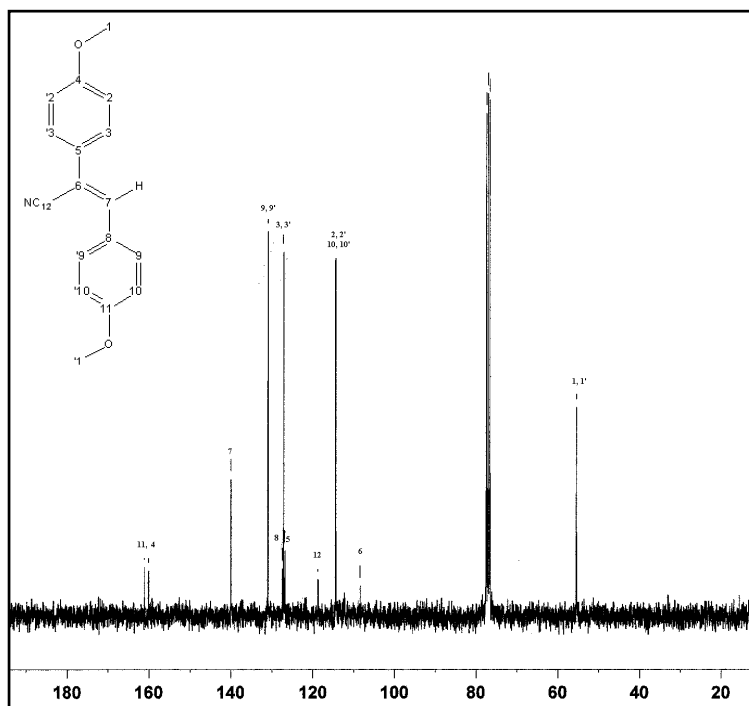
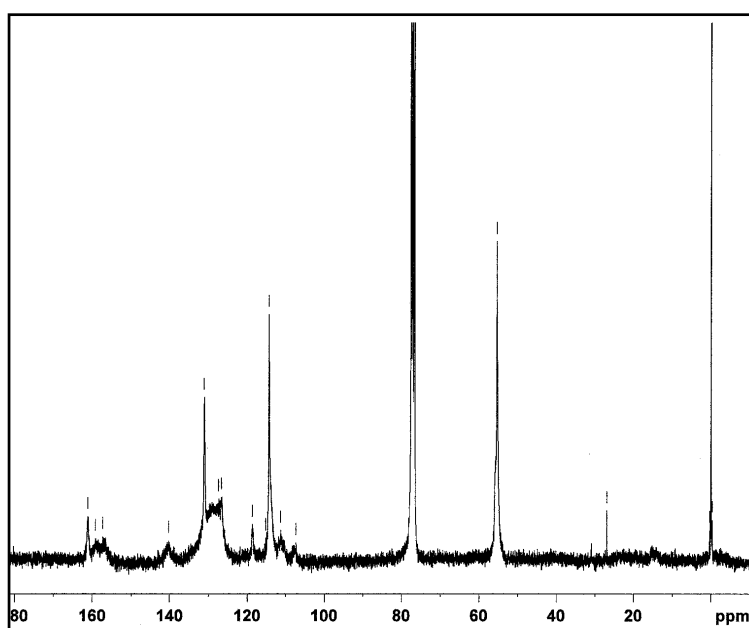
### 3.1. Synthesis and Characterization

We prepared the oligomer (OMPA) by the electrolysis of (4-methoxy phenyl) acetonitrile at a controlled potential of 1.8 V as described in the experimental section. The results of osmometry and gel permeation chromatography analyses indicated that the average chain length was about 5 units [26]. Afterward, OMPA was subjected to a chemical modification via the Knoevenagel condensation with the 4-methoxybenzaldehyde (Scheme 1). The resulting material was analyzed by NMR and FTIR spectroscopy. To analyze the recorded spectra and assign different signals, we prepared the (Z)-2,3-bis(4-methoxyphenyl) acrylonitrile (BMPA) which will serve as a model.

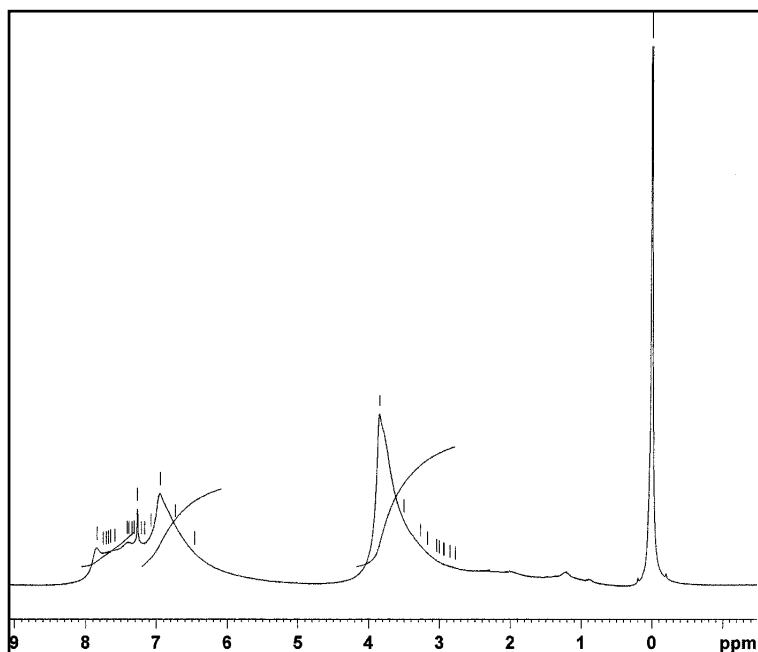
**Scheme 1.** OBMPA synthesis.



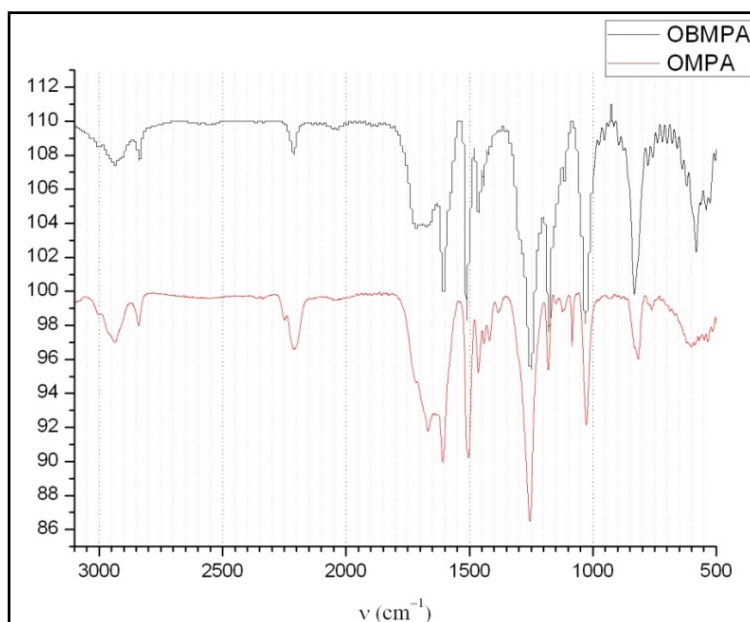
In Figures 1 and 2 we give the  $^{13}\text{C}$  NMR spectra of BMPA and OBMPA, respectively. They revealed that OMPA was partially modified by the Knoevenagel reaction. In fact, the signals appearing at 140.2 and 107.3 ppm in the OBMPA spectrum correspond to the ethylenic carbons resulting from the chemical modification. On the other hand, the presence of a signal at 26.9 (Figure 2), corresponding to unreacted benzylic carbons, evidenced incomplete modification. It should be noted that signals located around 111 ppm and 130 ppm were assigned to the quaternary carbons resulting from the C-C inter-ring bond in the oligophenylene structure.

**Figure 1.**  $^{13}\text{C}$  NMR spectra of BMPA.**Figure 2.**  $^{13}\text{C}$  NMR spectra of OBMPA.

In the  $^1\text{H}$  NMR spectra of OBMPA, given in Figure 3, we detected two broad signals. The first appeared around 3.8 ppm and corresponded to methoxylic and to unreacted benzylic protons. The second signal, recorded between 6.8 and 8 ppm, was assigned to aromatic and vinylic protons. To appreciate the modification ratio, we compared the integrations of the methoxylic/benzylic proton peak and the aromatic/vinylic proton peak. A value around 70% was calculated, demonstrating partial modification, probably caused by steric hindrance induced by the modified chains.

**Figure 3.**  $^1\text{H}$  NMR spectra of OBMPA.

The recorded FTIR spectra for OMPA and OBMPA are illustrated in Figure 4. It can be noted that both spectra possess almost the same absorption bands. The most important bands are grouped in Table 1.

**Figure 4.** FTIR spectra of OBMPA (top) and OMPA (bottom).**Table 1.** Group frequency assignments for the main infrared bands observed in OMPA and OBMPA spectra.

Vibration	Aromatic ring C-H stretching	Methyl group C-H stretching	Nitrile C≡N stretching	Aromatic ring C=C stretching	Methoxy C-O-C
$\nu(\text{cm}^{-1})$	3,100	2,900	2,258	1,609, 1,512, 1,470	1,250, 1,029

However, we detected few modifications in the OBMPA spectrum. In fact, the intensity of the band appearing at  $858\text{ cm}^{-1}$ , typical of C-H out-of-plane vibration, was enhanced because of the introduction of the 1,4 disubstituted benzene in the 4-methoxy cyanostyryl moiety. In addition, the form of the band appearing at  $2258\text{ cm}^{-1}$ , corresponding to the nitrile stretching, probably changed due to the bond conjugation with the rest of the molecular structure.

### 3.2. Electrochemical Study

Cyclic voltammetric measurements were performed using a three-electrode cell setup with 0.1 M tetrabutylammonium tetrafluoroborate ( $\text{Bu}_4\text{NBF}_4$ ) as a supporting electrolyte in degassed acetonitrile. We studied the electrochemical behavior of the oligomers to understand their electrochemical stability in p and n-doped states. Figures 5 and 6 illustrate the cyclic voltammograms of BMPA and OBMPA, respectively. During the first anodic scan (Figure 5), BMPA exhibits an irreversible oxidation peak at around 1.38V which is 0.3 V lower than that of MPA [26], clearly indicating the effect of the 4-methoxy cyanostyryl as a donor unit. Moreover, an irreversible reduction peak was detected at about  $-1.2\text{ V}$  evidencing the effect of the conjugated nitrile group, facilitating the reduction step by its electron-withdrawing nature. The peaks' irreversibility indicate the short lifetime of the radical ions formed during the electrochemical processes. The cyclic voltammogram of OBMPA also exhibits irreversible anodic and cathodic responses. However, no clear peaks were recorded. This result could be explained by the presence of oligomer chains with different lengths and by a slow electron transfer processes. Nevertheless, the electrochemical gap, related to the highest occupied (HOMO) and lowest unoccupied (LUMO) molecular orbitals, can be estimated by calculating the difference between the onset of electron injection and hole injection under experimental conditions. We note that both anodic and cathodic processes occur at lower potentials than for BMPA. In fact, the extension of the electronic delocalization, over the molecular structure of the modified oligomer, stabilizes the electrogenerated radical ions. The calculated electrochemical band gap of OBMPA was found to be 2 eV.

**Figure 5.** Oxidation and reduction voltammogram of BMPA performed in acetonitrile,  $\text{NBu}_4\text{BF}_4$  0.1 M;  $C = 10^{-3}\text{ M}$ ;  $\nu = 100\text{ mVs}^{-1}$  on platinum disc ( $d = 2\text{ mm}$ ).

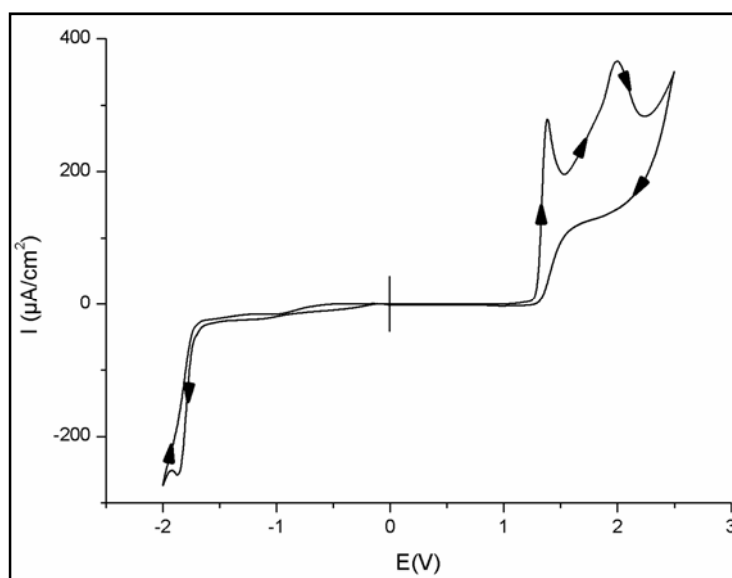
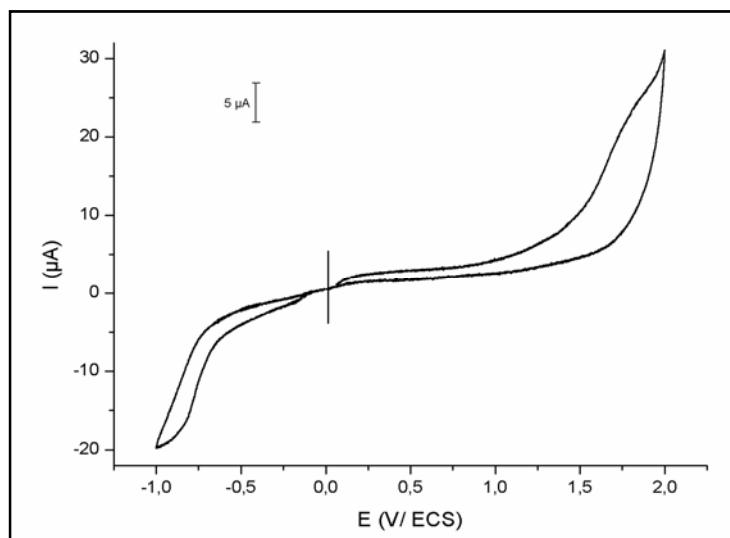


**Figure 6.** Oxidation and reduction voltammogram of OBMPA performed in acetonitrile, NBu<sub>4</sub>BF<sub>4</sub> 0.1 M;  $C = 10^{-3}$  M;  $\nu = 20$  mVs<sup>-1</sup> on platinum disc (d = 2 mm).

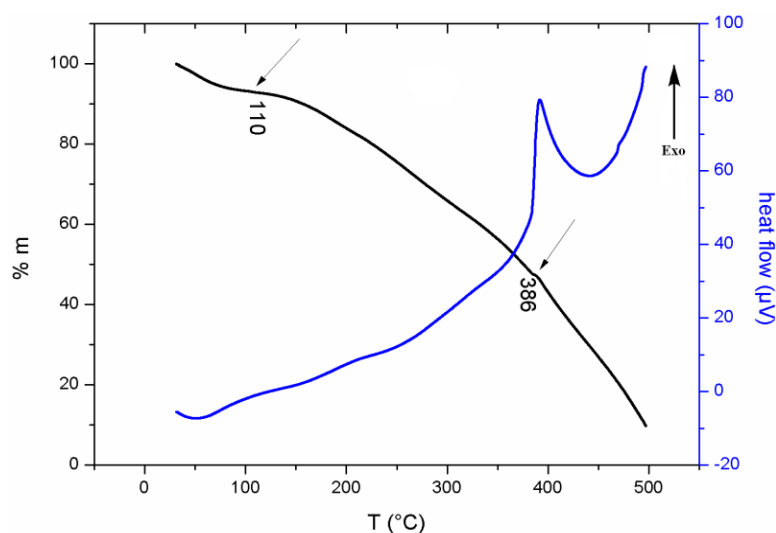


Besides, we calculated the HOMO and the LUMO energies as described in the experimental section. We estimated  $E_{\text{HOMO}}$  and  $E_{\text{LUMO}}$  to be  $-5.7$  and  $-3.7$  eV, respectively.

### 3.3. Thermal Study

OBMPA thermal stability was investigated by TGA and DTA. The obtained results are shown in Figure 7. It should be noted that a small weight loss (<10%), most probably related to evaporation of the residual solvents used during the oligomer preparation and purification, was observed from 80 °C to 120 °C. The results of differential thermal analysis showed that a slow exothermic phenomenon took place from 150 °C to 391 °C when an accentuated peak was observed. The corresponding weight loss exceeded 50%. This phenomenon could be attributed to the degradation of phenylstyryl pendant chains. This assumption was supported by the lower thermal stability of the modified oligomer relatively to OMPA [26]. Finally, a faster degradation was observed from 450 °C, corresponding to the polyphenylene backbone degradation as previously described [27].

**Figure 7.** TGA and TDA thermogram of OBMPA under Nitrogen.



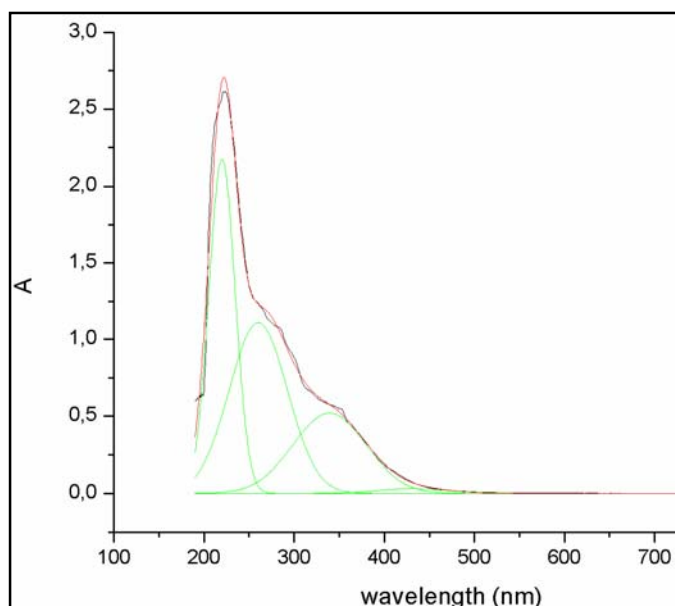
### 3.4. Optical Properties

The optical absorption spectroscopy enables fundamental information on the properties of absorption to be provided, especially in the case of molecules very absorbent in the UV-visible as well as in conjugated polymers.

#### 3.4.1. Optical Absorption

The optical absorption spectrum performed on OBMPA in chloroform solution is shown in Figure 8. From this spectrum we can immediately deduce that the solution of OBMPA absorbs in UV and near UV ranges with a strong absorption band located at 220 nm.

**Figure 8.** UV-vis absorption spectra of OBMPA in chloroform solution (—), deconvolution of UV-vis absorption spectra of OBMPA into compounds of Lorentzian profile (—).



When compared to the OMPA spectrum, a new band appeared at around 350 nm. This band can be explained by the extension of the electronic delocalization over the oligomer after the chemical modification. The onset  $\lambda_{\text{onset}}$  of the OBMPA optical absorption spectrum (Figure 8) is estimated to be at 450 nm (2.75 eV). This indicates that the band gap of OBMPA is smaller compared to that reported for the unmodified oligomer (400 nm; 3.1 eV) [26]. Note that this value is different from the electrochemical gap previously obtained. This result could be explained by the fact that the optical electron transition leads to the formation of excited states, whereas electrochemical reduction/oxidation are reactions generating species in ground states. Indeed, the electro-generation of a radical cation or radical anion in solution involves other thermodynamic (solvation...) and kinetic effects. In fact, it is expected that the onset potential will be lowered owing to fast chemical reactions following electron transfer inducing kinetic instability of the primarily generated radical ions.

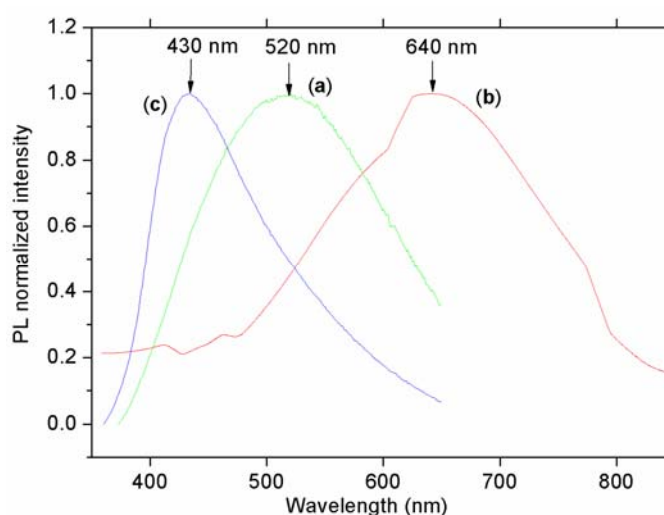
### 3.4.2. Photoluminescence

The steady state PL is widely used to provide fundamental information on the photophysical properties.

#### *Steady State PL*

Figure 9 displays the steady state PL spectra carried out on an OBMPA thin film and in chloroform solution. The PL spectrum of OBMPA in solution (Figure 9(a)) presents a maximum emission at 520 nm whereas that of the spectrum of OBMPA thin film spectrum (Figure 9(b)) is red-shifted by a value of 120 nm. This red-shift of emission in solid-state OBMPA suggests an extent of conjugation related to the improvement of the macromolecular organization with respect to the parallel direction of the substrate. Contrary to the OBMPA film, the OBMPA solution has individual polymer chains coiled to varying degrees which interrupt the conjugation. In this case, the short and isolated conjugated segments are predominant, inducing a decrease of the effective conjugation length. This result shows how the morphology plays a crucial role in the emission of organic compounds. An additional spectrum of OMPA in chloroform solution has been recorded for comparison (Figure 9(c)). It presents a maximum emission blue shift of 90 nm with respect to OBMPA in solution. This result is well explained by the presence 4-methoxy cyanostyryl pendant chains in OBMPA. These lateral groups increase the degree of delocalization of  $\pi$  electrons on the carbon atoms of the oligomer backbone which are responsible for the conjugation. This case shows how the chemical nature of the substituent group can impact the conjugation of polymer.

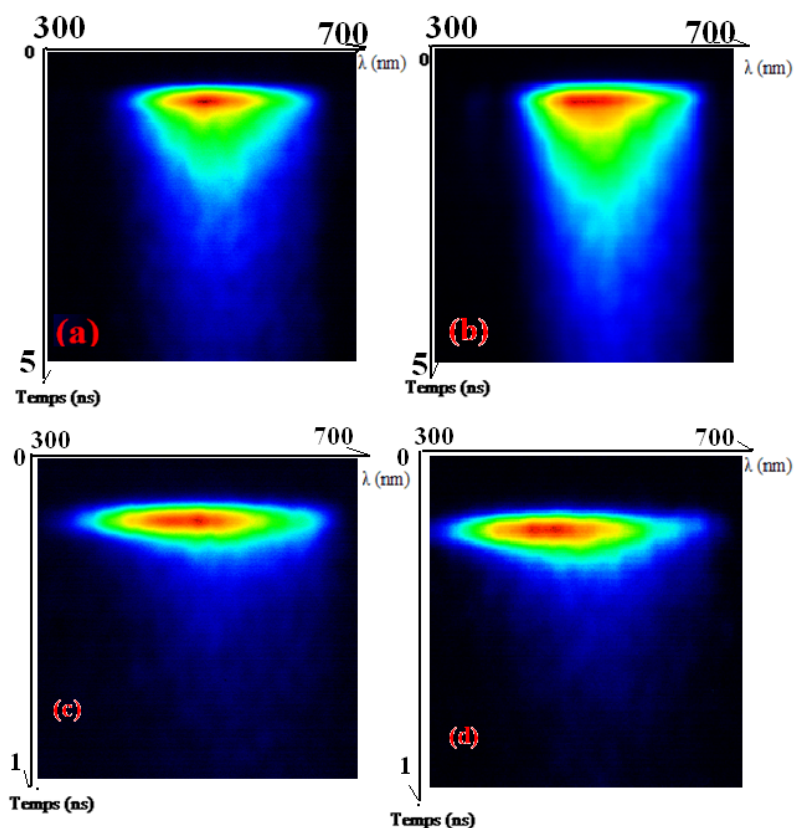
**Figure 9.** Steady state PL spectra of OBMPA in solution (a) and (b) thin films and OMPA in solution (c); (excitation wavelength 350 nm).



#### *Time-Resolved Photoluminescence (TR-PL)*

This technique provides vital information on the dynamics of charge carriers and/or excitons created after photoexcitation, which are responsible for the emission of light in organic materials. The lifetime and migration of these species is strongly dependent on the material morphology at the microscopic and mesoscopic scales.

**Figure 10.** 3D-maps TR-PL of OBMPA (a) solution, (b) solution, (c) thin film and of OMPA, (d) thin film.



3D-maps of TR-PL in false colors on both oligomers are presented in Figure 10 using the excitation energy 4.64 eV (267 nm). Colors going from blue to red represent the increase of the PL intensity. From these 3D-maps, we can deduce the normalized PL decay dynamics on a logarithm scale within a temporal window of 0–5 ns for the oligomers in solution (Figure 10(a,b)) and within a temporal window of 0–1 ns for the oligomers in solid state (Figure 10(c,d)).

We analyzed the TR-PL decays for both oligomers in order to obtain information on the nature and the lifetime of the photoexcitations generated in the excited states.

A single monoexponential fit cannot reproduce these data for the temporal window of 0–1 ns. This suggests the presence of several decay mechanisms. In fact, the kinetics are well reproduced with two coupled exponential decays convoluted with the contribution of apparatus function involving a Gaussian laser pulse.

We used a simple model with two excited levels [27]. The populations,  $n_1$  and  $n_2$ , of the excited states levels 1 and 2 have respective lifetimes  $\tau_1$  and  $\tau_2$ . Photogenerated charges populating the higher energy level 1 migrate toward defects and fast relax on the lower energy state 2 with lifetime  $\tau_1$ . Over a longer period of time, the photogenerated charges on level 2 are less mobile and consequently survive longer with a slower time constant  $\tau_2$ . The two populations include photogenerated charges recombining radiatively and nonradiatively.

We define below (Equation (1)) an average decay time  $\tau_{mean}$  in order to show the average trend of the photogenerated charge migration time.

$$\tau_{mean} = \frac{A_1\tau_1^2 + A_2\tau_2^2}{A_1\tau_1 + A_2\tau_2} \tag{1}$$

For clarity, the weight corresponding to the relative population of photogenerated charges contributing to each of the decay times ( $A_i, \tau_i$ ) is calculated by the following formula:

$$P_i(\%) = \frac{A_i\tau_i}{\sum A_i\tau_i} \tag{2}$$

Results are summarized in Table 2 where  $P_i$  is reported in parentheses for each decay component. The TR-PL normalized intensity decay (Figures 11 and 12) fit very well with two coupled exponential decays as previously reported [27]. The solid lines represent the curve fits.

**Figure 11.** Integrated TR-PL decays of (a) OMPA and (b) OBMPA in chloroform solution.

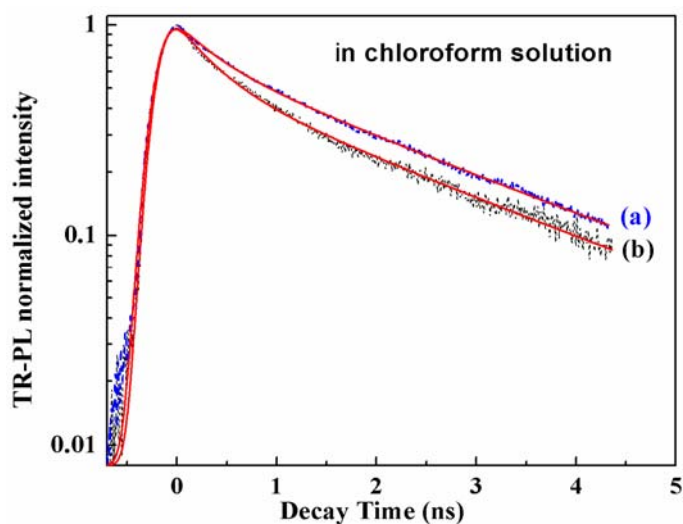


**Figure 12.** Integrated TR-PL decays of (a) OMPA and (b) OBMPA in solid state thin film.

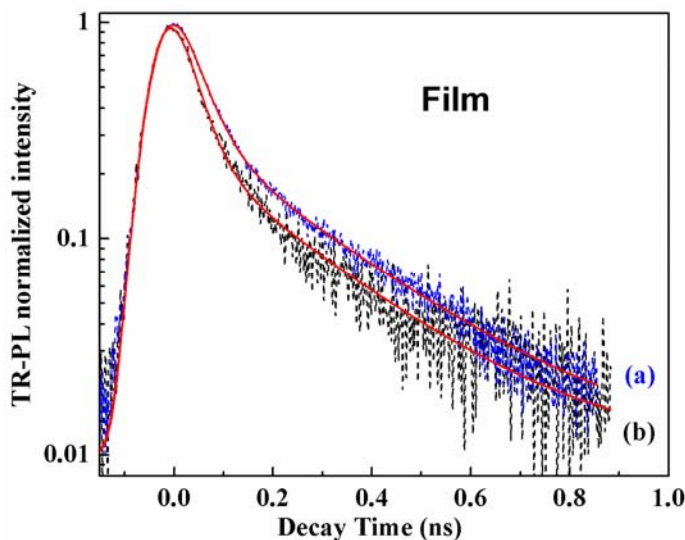


**Table 2.** Decay constant times ( $\tau_1, \tau_2, \tau_{\text{mean}}$ ), the pre-exponential factor ( $A_1, A_2$ ) and percentage contributions  $P_1$  and  $P_2$  to emission levels 1 and 2.

Samples	$\tau_1$ (ns) $P_1\%$ ( $A_1$ )	$\tau_2$ (ns) $P_2\%$ ( $A_2$ )	$\tau_{\text{mean}}$ (ns)
OBMPA (solution)	0.38 31 (9.5)	2.22 68 (3.6)	1.36
OBMPA (film)	0.034 56 (15.2)	0.235 43 (1.67)	0.11
OMPA (solution)	0.4 26 (8.7)	2.32 74 (4.2)	1.82
OMPA (film)	0.041 55 (14.6)	0.25 45 (2)	0.136

From Figures 11 and 12, it is clear that in solutions and in solid state (films), the PL lifetime of OMPA is higher than that of OBMPA. This is confirmed by the respective values of  $\tau_{\text{mean}}$  obtained from Table 2. This result is explained by the presence of the 4-methoxy cyanostyryl pendant chains in OBMPA. These lateral groups increase the degree of delocalization of the  $\pi$  electrons, therefore promoting the photoexcitation migration on conjugated segments with an increase of trapping probability for OBMPA. From Figures 11 and 12, we can see that both oligomers have a faster PL decay in thin films than in solutions. This is confirmed by the respective values of  $\tau_{\text{mean}}$  and can be explained by the difference of morphology of samples in solution or in film already discussed in Section 3.4. Indeed, the action of a good solvent in solution enables oligomer chains to be isolated in order to minimize interchain interactions. This mechanism is opposite to the case of films where the polymer chains are closer to each other, inducing strong interchain interaction [28,29]. On going from solution to film the migration of photoexcitations is therefore favored and provides a faster decay channel.

#### 4. Conclusions

In this study we showed that the Knoevenagel condensation of a functionalized oligophenylene (OMPA) with substituted benzaldehydes can be used for controlling the optical properties of the resulting material. The OMPA was obtained by the electrochemical oxidation of (4-methoxy phenyl) acetonitrile. The chemical modification, performed with the 4-methoxy benzaldehyde, led to a partially modified (70%) oligophenylene processing a 4-methoxy cyanostyryl moiety as a pendant chain. The material obtained was characterized by various spectroscopic techniques: photoluminescence, NMR, FTIR, and UV. The optical study revealed that, in solution, the modified oligomer exhibited an emission at 520 nm, taking place 100 nm higher than the non-modified material and that the optical gap changed from 3.1 eV to 2.75 eV. In the solid state, this emission was again red-shifted by 120 nm because of interaction between the oligomer chains. The transient photoluminescence study showed that the intensity decays of both oligomers are fit very well with two coupled exponential decays. Moreover, the lifetimes of the photo-generated species were shortened by the conjugation extension in the modified oligomer and by the inter-chain interactions in the solid state.

## Acknowledgments

This research was supported by the Ministry of Higher Education and Scientific Research, Tunisia.

## References

1. *Conjugated Polymers: Theory, Synthesis, Properties, and Characterization*, 3rd ed.; Skotheim, T.A., Reynolds, J., Eds.; CRC Press, Taylor & Francis Group: Boca Raton, FL, USA, 2007.
2. Wallace, G.G.; Sprinks, G.M.; Kane-Maguire, L.A.P.; Teasdale, P.R. *Conductive Electroactive Polymers: Intelligent Materials Systems*, 2nd ed.; CRC Press, Taylor & Francis Group: Boca Raton, FL, USA, 2009.
3. Gunes, S.; Neugebauer, H.; Sariciftci, N.S. Conjugated polymer-based organic solar cells. *Chem. Rev.* **2007**, *107*, 1324–1338.
4. Roncali, J. Conjugated poly(thiophenes): Synthesis, functionalization, and applications. *Chem. Rev.* **1992**, *92*, 711–738.
5. Higgins, S.J. Conjugated polymers incorporating pendant functional groups: Synthesis and characterization. *Chem. Soc. Rev.* **1997**, *26*, 247–257.
6. Leclerc, M.; Faid, K. Electrical and optical properties of processable polythiophene derivatives: Structure-property relationships. *Adv. Mater.* **1997**, *9*, 1087–1094.
7. Swager, T.M. The molecular wire approach to sensory signal amplification. *Acc. Chem. Res.* **1998**, *31*, 201–207.
8. Cravino, A.; Zerza, G.; Maggini, M.; Bucell, S.; Svensson, M.; Andersson, M.R.; Neugebauer, H.; Sariciftci, N.S. A novel polythiophene with pendant fullerenes: Toward donor/acceptor double-cable polymers. *Chem. Commun.* **2000**, *24*, 2487–2488.
9. Cihaner, A.; Önal, A.M. Synthesis of a regular polymer containing pseudo-polyether cages. *Synth. Met.* **2005**, *150*, 39–45.
10. Roncali, J. Synthetic principles for bandgap control in linear  $\pi$ -conjugated systems. *Chem. Rev.* **1997**, *97*, 173–206.
11. Wang, H.-J.; Chan, L.-H.; Chen, C.-P.; Lin, S.-L.; Lee, R.-H.; Jeng, R.-J. Bulky side-chain density effect on the photophysical, electrochemical and photovoltaic properties of polythiophene derivatives. *Polymer* **2011**, *52*, 326–338.
12. Chen, J.-C.; Liu, Y.-C.; Ju, J.-J.; Chiang, C.-J.; Chern, Y.-T. Synthesis, characterization and hydrolysis of aromatic polyazomethines containing non-coplanar biphenyl structures. *Polymer* **2011**, *52*, 954–964.
13. Karsten, B.P.; Bijleveld, J.C.; Viani, L.; Cornil, J.; Gierschner, J.; Janssen, R.A.J. Electronic structure of small band gap oligomers based on cyclopentadithiophenes and acceptor units. *J. Mater. Chem.* **2009**, *19*, 5343–5350.
14. Paul-Roth, C.; Rault-Berthelot, J.; Simonneaux, G.; Poriel, C.; Abdalilah, M.; Letessier, J. Electroactive films of poly(tetraphenylporphyrins) with reduced bandgap. *J. Electroanal. Chem.* **2006**, *597*, 19–27.
15. Rault-Berthelot, J.; Paul-Roth, C.; Poriel, C.; Juillard, S.; Ballut, S.; Drouet, S.; Simonneaux, G. Comparative behaviour of the anodic oxidation of mono-, di- and tetra-arylporphyrins: Towards new electroactive materials with variable bandgaps. *J. Electroanal. Chem.* **2008**, *623*, 204–214.

16. Grimsdale, A.C.; Müllen, K. Oligomers and polymers based on bridged phenylenes as electronic materials. *Macromol. Rapid. Commun.* **2007**, *28*, 1676–1702.
17. Poriel, C.; Liang, J.-J.; Rault-Berthelot, J.; Barrière, F.; Cocherel, N.; Slawin, A.M.Z.; Horhant, D.; Virboul, M.; Alcaraz, G.; Audebrand, N.; Vignau, L.; Huby, N.; Wantz, G.; Hirsch, L. Dispirofluorene—indenofluorene derivatives as new building blocks for blue organic electroluminescent devices and electroactive polymers. *Chem. Eur. J.* **2007**, *13*, 10055–10069.
18. Yildirim, A.; Tarkuc, S.; Aka, M.; Toppare, L. Syntheses of electroactive layers based on functionalized anthracene for electrochromic applications. *Electrochim Acta.* **2008**, *53*, 4875–4882.
19. Manhart, S.A.; Adachi, A.; Sakamaki, K.; Okita, K.; Ohshita, J.; Ohno, T.; Hamaguchi, T.; Kunai, A.; Kido, J. Synthesis and properties of organosilicon polymers containing 9,10-diethynylantracene units with highly hole-transporting properties. *J. Organomet. Chem.* **1999**, *592*, 52–60.
20. Killian, J.G.; Gofer, Y.; Sarker, H.; Poehler, T.O.; Searson, P.C. Electrochemical synthesis and characterization of a series of fluoro-substituted phenylene-2-thienyl polymers. *Chem. Mater.* **1999**, *11*, 1075–1082.
21. Lu, Y.; Chena, H.; Houa, X.; Hub, X.; Ng, S.-C. A novel low band gap conjugated polymer based on N-substituted dithieno[3,2-b:2',3'-d]pyrrole. *Synth. Met.* **2010**, *160*, 1438–1441.
22. Koyuncua, F.B.; Koyuncub, S.; Ozdemir, E.A. A Novel donor-acceptor polymeric electrochromic material containing carbazole and 1,8-naphthalimide as subunit. *Electrochim. Acta.* **2010**, *55*, 4935–4941.
23. Pan, X.Y.; Liu, S.P.; Chan, H.S.O.; Ng, S.C. Novel fluorescent carbazolyl-pyridinyl alternating copolymers: Synthesis, characterization, and properties *Macromolecules.* **2005**, *38*, 7629–7635.
24. Janietz, S.; Bradley, D.D.C.; Grell, M.; Gieberler, C.; Inbasekaran, M. Electrochemical determination of the ionization potential and electron affinity of poly(9,9-dioctylfluorene). *Appl. Phys. Lett.* **1998**, *73*, 2453–2455.
25. Bredas, J.L.; Silbey, R.; Boudreaux, D.S.; Chance, R.R. Chain-length dependence of electronic and electrochemical properties of conjugated systems: Polyacetylene, polyphenylene, polythiophene, and polypyrrole. *J. Am. Chem. Soc.* **1983**, *105*, 6555–6559.
26. Ben Amor, S.; Haj Said, A.; Chemek, M.; Ayachi, S.; Massuyeau, F.; Wéry, J.; Alimi, K.; Roudesli, S. Electrosynthesis and characterization of oligophenylene deriving from 4-(methoxyphenyl) acetonitrile. *J. Mol. Struct.* **2012**, doi: 10.1016/j.molstruc.2012.03.050.
27. Massuyeau, F.; Faulques, E.; Lefrant, S.; Majdoub, M.; Ghedira, M.; Alimi, K.; Wéry, J. Photoluminescence properties of new PPV derivatives. *J. Luminesc.* **2011**, *131*, 1541–1544.
28. Haj Said, A.; Ayachi, S.; Issaoui, C.; Wéry, J.; Alimi, K. Optical and vibrational studies on single walled carbon nanotubes/short oligo-para-methoxy-toluene composite. *J. Appl Polym. Sci.* **2011**, *122*, 1889–1897.
29. Chemli, M.; Haj Said, A.; Jaballah, N.; Fave, J.-L.; Majdoub, M. Synthesis and characterization of new electroluminescent poly(p-phenylene) derivative. *Synth. Met.* **2011**, *161*, 1463–1468.